Ferro- and antiferro-magnetism in (Np, Pu)BC

T. Klimczuk; A. B. Shick; A. L. Kozub; J.-C. Griveau; E. Colineau; M. Falmbigl; F. Wastin; P. Rogl

Check for updates

CrossMark

View Online

Export Citation

Ferro- and antiferro-magnetism in (Np, Pu)BC

T. Klimczuk,[1,2,a] A. B. Shick,[3] A. L. Kozub,[2,3] J.-C. Griveau,[1] E. Colineau,[1]
M. Falmbigl,[4] F. Wastin,[1] and P. Rogl[4,b]

[1]*European Commission, Joint Research Centre (JRC), Institute for Transuranium Elements
(ITU), Postfach 2340, 76125 Karlsruhe, Germany*
[2]*Faculty of Applied Physics and Mathematics, Gdansk University of Technology,
Narutowicza 11/12, 80-233 Gdansk, Poland*
[3]*Institute of Physics, ASCR, Na Slovance 2, CZ-18221 Prague, Czech Republic*
[4]*Institute for Physical Chemistry, University Vienna, Währingerstrasse 42,
A-1090 Wien, Austria*

Two new transuranium metal boron carbides, NpBC and PuBC, have been synthesized. Rietveld refinements of powder XRD patterns of {Np,Pu}BC confirmed in both cases isotypism with the structure type of UBC. Temperature dependent magnetic susceptibility data reveal antiferromagnetic ordering for PuBC below T_N = 44 K, whereas ferromagnetic ordering was found for NpBC below T_C = 61 K. Heat capacity measurements prove the bulk character of the observed magnetic transition for both compounds. The total energy electronic band structure calculations support formation of the ferromagnetic ground state for NpBC and the antiferromagnetic ground state for PuBC. © 2015 Author(s). All article content, except where otherwise noted, is licensed under a Creative Commons Attribution 3.0 Unported License.
[http://dx.doi.org/10.1063/1.4913564]

The actinoid compounds provide complex physics often difficult to understand. It is due to the nature of the 5f states, which causes a wide variety of unexpected behaviors, such as unconventional superconductivity, Kondo effect and heavy fermion ground state, valence fluctuations, and long-range magnetic ordering.[1–4] The radioactive nature and high toxicity of these materials make handling and experiments difficult and very expensive. Therefore, only a few laboratories in the world are able to synthesize and study new actinide based compounds.

The actinoid elements, which have radii similar to the lanthanoids and are usually trivalent, can often replace the lanthanoid in a compound without changing its crystal structure. In contrast to the 4f electrons of the lanthanoids, the 5f electrons of the light actinoid elements reveal itinerant character. Therefore, although the existence of a lanthanoid compound allows us to design an actinoid analogue, its physical properties will be difficult to predict. Recent examples are the transuranic based iron oxypnictides: NpFeAsO (Ref. 5) and PuFeAsO (Ref. 6), the analogues of the rare earth RFeAsO high-temperature superconductors. Itinerant character of the 5f electrons causes a big change in the physical properties of NpFeAsO and PuFeAsO, i.e., lack of the spin density wave condensation and structural phase transition that are present in the parent RFeAsO compounds.

The compounds containing boron and carbon in their crystal structure very often reveal interesting physics. For example, a large family of rare-earth boron-carbide superconductors (Refs. 7 and 8) was intensively studied due to their unique interplay of superconductivity and magnetism.[9] Physical and chemical properties of uranium based carbides, borides, and boron-carbides are of special interest because UC may serve as a dense fuel for nuclear reactors controlled by "B$_4$C"-rods.

The existence of two actinoid based boron-carbide families has been reported (Refs. 10 and 11). The compounds from the first family, AnB$_2$C (An-actinoid i.e., Th, U, Np, Pu), crystallize

---

[a]Author to whom correspondence should be addressed. Electronic mail: tomasz.klimczuk@pg.gda.pl; Fax: +43 1 4277 524 56 and +48 58 347 2821.
[b]E-mail: peter.franz.rogl@univie.ac.at

with a unique rhombohedral structure type, ThB_2C (space group $R\bar{3}m$), with some resemblance to the simple hexagonal AlB_2-type. Their magnetic properties vary from temperature independent paramagnetism observed for α-UB_2C (Ref. [12]) and PuB_2C (Ref. [13]), through antiferromagnetism to weak ferromagnetism observed for β-UB_2C (Refs. [12], [14], and [15]) and PuB_2C (Ref. [13]), respectively. The second family, actinoid metal monoboro-monocarbides form, with two different structure types, i.e., a unique structure type for the larger Th-atom deriving from αMoB-type, whereas the smaller atoms U, Np, Pu adopt the UBC-type derived from the CrB-type structure.[16,17] UBC alloys were reported to be temperature independent paramagnetic[12] (TIP) in the temperature range from 100 to 1100 K with the low temperature tail below 80 K being due to traces of ferromagnetic ß-UB_2C.

In this paper, we report on the crystal structure and physical properties of NpBC and PuBC, two members of the AnBC family. Band structure calculations (LSDA+U) support the experimentally observed ferromagnetic (FM) state for NpBC and the antiferromagnetic (AFM) ground state for PuBC.

Polycrystalline ingots were obtained by arc melting stoichiometric amounts of the constituent elements under Zr-gettered high purity argon on a water-cooled copper hearth. Starting materials were used in the form of pieces as supplied by Merck AG (boron and graphite), and electrorefined 3N-neptunium (^{237}Np, $T_{1/2} = 2.14 \times 10^6$ y) and 3N6-plutonium (^{239}Pu, $T_{1/2} = 2.4 \times 10^4$ y) metal supplied by Los Alamos National Laboratory. In order to ensure homogeneity, the arc-melted buttons were turned over and remelted 3 times, with weight losses below 0.5%. The neptunium isotope does not reveal a visible problem of self-induced defects and structural disorder caused by the α-decay of the Np nuclei (ageing effect). On the contrary, the structural, magnetic, and electronic properties of plutonium containing compounds can be significantly affected by ageing.[18] Therefore, physical properties of PuBC were measured promptly after annealing. The sample quality was checked by X-ray powder diffraction data (Cu K_α radiation) collected on a Bragg-Brentano Siemens D500 and D8-diffractometer using a step size in 2Θ of 0.02°. The diffraction patterns were analyzed by a Rietveld-type profile refinement method using the Fullprof program.[19] Bulk magnetic measurements were performed on encapsulated chunks using a Quantum Design MPMS7-SQUID in fields up to 7 T and in the temperature range from 2 to 300 K. Specific heat data were measured by using the relaxation method (Quantum Design PPMS) in the temperature range from 2 to 300 K (up to 9 T). Since our compounds contain highly radioactive Np or Pu, small samples with a mass below 5 mg were covered/wrapped in heat conducting STYCAST 2850 FT resin. The mass of the resin was known and the raw experimental data have been corrected for this additional heat capacity contribution.

All DFT(Density Functional Theory) calculations make use of the in-house implementation[20,21] of the full-potential linearized augmented plane wave (FP-LAPW) method. This FP-LAPW version includes all relativistic effects: scalar-relativistic and spin-orbit coupling (SOC). The radii of the atomic muffin-tin (MT) spheres are set to 2.7 a.u. (Np, Pu) and 1.3 a.u. (B, C). The basis set size is characterized by the parameter $R_{Np} \times K_{max} = 8.1$ and the Brillouin zone is sampled with 729 k points. The magnetization is aligned along the c-axis (direction of the shortest An-An bonds).

Rietveld refinements of the X-ray patterns of the well crystallized alloys of {Np,Pu}BC unambiguously revealed crystal symmetry, systematic extinctions, and cell size as characteristic for the UBC-type (see Table I). Intensity data refinement with isotropic thermal parameters for all atoms showed full occupation of all atom sites in agreement with the formula AnBC. The absence of supercell reflections confirmed isotypism with the structure type of UBC[17] presented in Figure 1. Whereas metal-nonmetal bonds essentially correspond to the sum of radii, metal-metal interaction (eight bonds for An-atoms) reveals two bonds at a distance slightly shorter than the sum of metal radii for CN = 12 (i.e., $d_{Np-Np} = 0.3380$ nm, $d_{Pu-Pu} = 0.3391$ nm, respectively) suggesting increased f-d hybridisation. Although there is no doubt about the metal arrangement in {Np,Pu}BC, Rietveld powder diffraction analysis is insufficient to yield details on the nonmetal bonding. Neutron diffraction studies on $UB_{1-x}C_{1+x}$ have clearly demonstrated[17] that the B-C sublattice (carbon-branched B-B chains with $d_{B-B} = 0.1874$ nm) in UBC adopts monoclinic symmetry in terms of space group $C12/m1$ as a *translationengleiche* crystallographic subgroup of *Cmcm*. Thereby the infinite C-branched boron chains are reduced to C-B-B-C groups ($d_{B-B} = 0.1706$ nm),

TABLE I. X-Ray Rietveld data[a] for NpBC and PuBC; UBC-type;[b] space group *Cmcm*; No. 63, Z = 4, origin at centre.

Compound	UBC	NpBC[c]	PuBC[d]
a (nm)	0.359 10(1)	0.359 13(1)	0.358 90(1)
b (nm)	1.198 80(4)	1.205 66(2)	1.202 10(3)
c (nm)	0.334 88(1)	0.338 03(1)	0.339 10(1)
Np/Pu in 4c (0,y,1/4)	y = 0.3610(1)	y = 0.3591(1)	y = 0.3592(1)
B in 4c	y = 0.0376(–)	y = 0.0376(–)	y = 0.0376(–)
C in 4c	y = 0.1643(–)	y = 0.1643(–)	y = 0.1643(–)
$R_I = \Sigma|I_o - I_c|/\Sigma I_o$	0.0801	0.0956	0.0705
$R_F = \Sigma|F_o - F_c|/\Sigma F_o$	0.0592	0.0575	0.0499
Interatomic distances An-An (nm)	U-2U 0.3349	Np-2Np 0.3380	Pu-2Pu 0.3391
	U-2U 0.3591	Np-2Np 0.3591	Pu-2Pu 0.3590
	U-4U 0.3622	Np-4Np 0.3605	Pu-4Pu 0.3604
	U-2U 0.3729	Np-2Np 0.3795	Pu-2Pu 0.3786

[a]Data collected at RT on D8; CuK$_\alpha$; 10° < 2Θ < 90°.
[b]Crystal structure data were standardized using program Typix.[32]
[c]Contains small amounts of NpB$_2$, AlB$_2$-type, a = 0.315 79(5) nm, c = 0.3978(1) nm.
[d]Contains small amounts of PuB$_2$C, ThB$_2$C-type, a = 0.654 49(2) nm, c = 1.078 12(4) nm.

which are loosely coupled via boron atoms at a distance of d_{B-B} = 0.2043 nm. A similar situation is expected for the non-metal sublattice in {Np,Pu}BC.

Transport properties for the AnBC compounds in comparison with AnB$_2$C are summarized in Table II. The temperature dependent magnetic susceptibility (χ) for NpBC, measured in an applied field of 1 T, is shown in Figure 2(a). At high temperature, $\chi(T)$ is almost temperature independent and below 80 K rapidly increases and saturates (field cooling) with χ_{sat} = 0.58 emu mol-Np^{-1}, or reaches the maximum with the same value of χ_{sat} (zero field cooling). The Curie temperature (T_C) was estimated as the inflexion point of the $\chi(T)$ curve, that is, the minimum of the first derivative $d\chi/dT$ as shown in Figure 2(b). By using this method, we obtained the Curie temperature T_C = 61 K. A ferromagnetic hysteresis loop (Figure 2(c)) is observed for NpBC at 2 K, with the remanent magnetization M_r = 1.14 μ_B/Np and the coercive field H_c = 0.75 T (600 kA/m). This high value of coercive field is in between the reported coercive field for sintered ferrite (240 kA/m) and cobalt rare earth compounds (720 kA/m).[22] It also well exceeds 10 kA/m, the widely used limit for a hard magnetic material.

The main panel of Figure 3 shows the temperature dependence of the zero-field-cooled susceptibility for PuBC and is typical for antiferromagnetic materials. The maximum of $\chi(T)$ at around 50 K is caused by the antiferromagnetic ordering of Pu ions. In order to obtain a precise value

TABLE II. Magnetic properties for AnB$_2$C and AnBC (An = U, Np, Pu).

	β -UB$_2$C[a]	NpB$_2$C	PuB$_2$C	UBC[b]	NpBC	PuBC
χ_0 (emu mol^{-1})	600×10^{-6}	531×10^{-6}	470×10^{-6c}	…	…	290×10^{-6}
Θ_p	+75 K	+27 K[d]	…	…	…	−56 K
$\mu_{eff/An-atom}$	1.45 μ_B	1.65 μ_B	…	…	…	1.37 μ_B
Magnetism	T_C = 75 K	T_N = 68 K	TIP	TIP	T_C = 61 K	T_N = 44 K
					Hard magnet	
γ (mJ mol^{-1} K^{-2})	34.7				11.9	31
θ_D (K)	314				395	305
The shortest An-An distance (nm)	0.3352	0.3363	0.3380	0.3349	0.3380	0.3391

[a]Reference 14.
[b]Reference 17.
[c]Possibly due to ferromagnetic impurities.
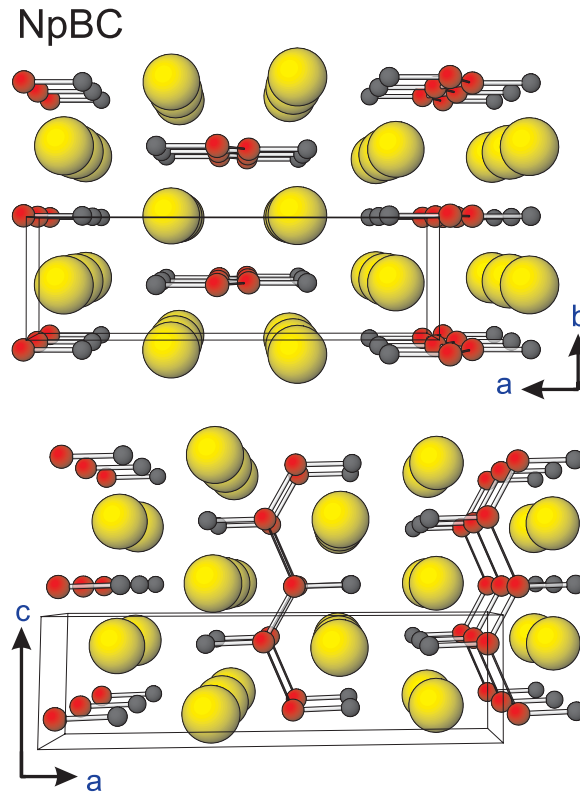[d]χ(300 K).

FIG. 1. Crystal structure of Np/PuBC in three-dimensional view (UBC-type). The yellow spheres represent the An atoms, whereas the red and dark spheres represent B and C atoms, respectively. The shortest distance between An-atoms is along the [001] direction.
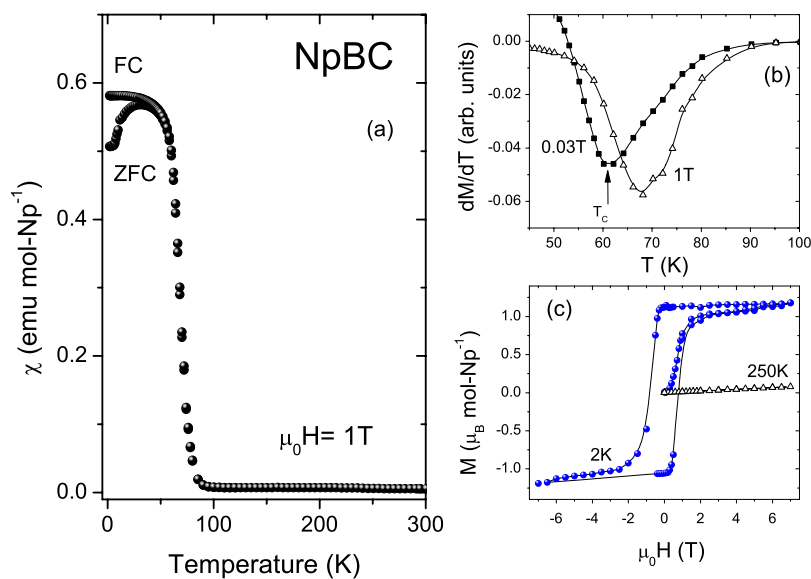

FIG. 2. Panel (a): zero-field-cooled magnetic susceptibility (solid circles) for NpBC measured under magnetic field $\mu_0 H = 1$ T. Panel (b): dM/dT vs. T in the vicinity of the Curie temperature (T_C) measured under fields of 0.03 (close squares) and 1 T (open triangles). Panel (c): M vs. H measured at 2 K (blue circles) and at 250 K (open triangles).
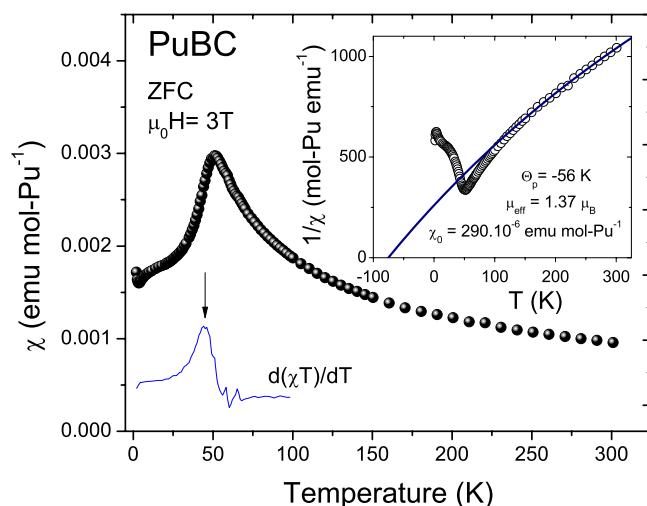
FIG. 3. Zero-field-cooled magnetic susceptibility (solid circles) and d(χT)/dT (solid line) for PuBC measured under magnetic field μ_0H = 3 T. The blue line shows d(χT)/dT in the same temperature range. The inset shows a Curie-Weiss fit (solid line) to the inverse susceptibility.

of the Nèel temperature, d(χT)/dT was plotted, and the Nèel temperature extracted for PuBC is T_N = 44 K. The high temperature part of the magnetic susceptibility can be fitted to the modified Curie-Weiss law, $\chi = \chi_0 + C/(T - \Theta_p)$, where χ_0 is the temperature independent susceptibility, C is the Curie constant, and Θ_P is the Weiss temperature. The fit to the equation is shown in the inset of Figure 3 as a solid line. The fitting parameters are μ_{eff} = 1.37 μ_B/Pu, Θ_p = −56 K, and χ_0 = 290 × 10^{-6} emu/mol. The μ_{eff} obtained is in very good agreement with the μ_{eff} observed for the PuFeAsO compound[6] and with the calculated effective moment for Pu^{+3} assuming intermediate coupling and zero crystal-field splitting (1.4 μ_B).[23] The negative value of the Curie Weiss temperature suggests the presence of antiferromagnetic interactions.

Heat capacity measurements for AnBC (An = Np, Pu) confirm a bulk phase transition for both NpBC and PuBC. The main panel of Figure 4 presents the temperature dependence of the specific heat for NpBC. A zero field measurement (μ_0H = 0 T) reveals a relatively week anomaly
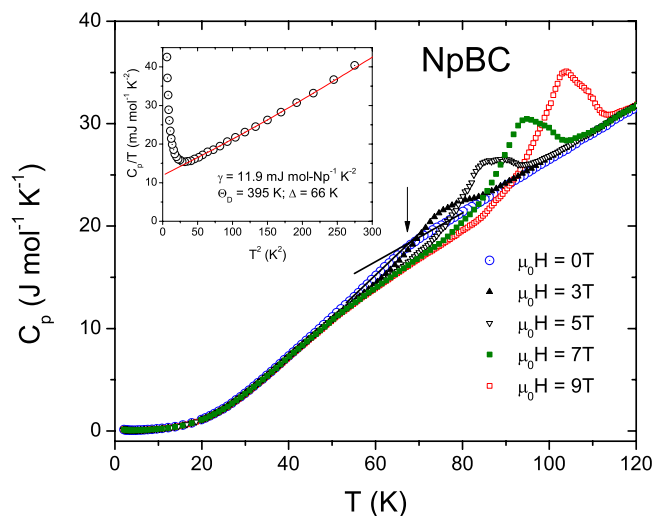

FIG. 4. Temperature dependence of the specific heat C_p for NpBC under magnetic fields from 0 to 9 T, presented in the form of C_p vs T (main panel) and C_p/T vs T^2 (inset). An arrow shows the Curie temperature T_C = 67 K estimated for μ_0H = 0 T. The red solid line in the inset represents a fit to the relation $C_p = \gamma T + \beta T^3 + \delta \exp(-\Delta/T)$.
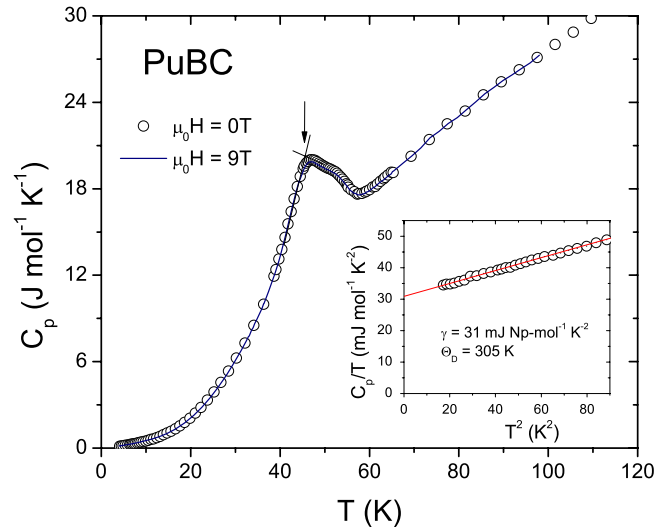
FIG. 5. Temperature dependence of the specific heat C_p for PuBC under a magnetic field of 0 T (open circles) and 9 T (solid line), presented in the form of C_p vs T (main panel) and C_p/T vs T^2 (inset). An arrow shows the Neel temperature $T_N = 45$ K. The red solid line in the inset represents a fit to the relation $C_p/T = \gamma + \beta T^2$.

that is associated with the ferromagnetic transition. The estimated Curie temperature ($T_C = 67$ K) is in good agreement with T_C derived from the magnetic susceptibility measurement ($T_C = 61$ K). On increasing magnetic fields, the anomaly becomes more pronounced and shifts towards higher temperature, i.e., applying a field of 9 T causes an increase by 35 K–102 K. The inset of Figure 4 presents C_p/T vs. T^2 and the solid line shows the fit to $C_p = \gamma T + \beta T^3 + \delta T^{3/2} \exp(-\Delta/T)$ yielding $\gamma = 11.9$ mJ Np-mol^{-1} K^{-2}, $\Theta_D = 395$ K, and $\Delta = 66$ K. The latter term in the fit is the low temperature magnon contribution to the C_p and Δ is the energy gap in the spin wave dispersion.[24] The low temperature upturn in C_p/T is caused by the Nuclear Schottky anomaly and is typical for neptunium based compounds, e.g., NpCoGa$_5$,[25] NpRh$_2$Sn,[26] and NpFeAsO.[5]

Temperature dependence of the specific heat for PuBC is shown in the main panel of Figure 5. A large anomaly with a maximum at 45 K is observed, in excellent agreement with the Nèel temperature derived from magnetic susceptibility measurement ($T_N = 44$ K). In contrast to NpBC, both the shape and the transition temperature do not depend on the applied magnetic field (open circles for 0 T and a solid line for 9 T). The specific heat anomaly is not perfectly λ-like; it has a small kink just above the maximum, suggesting a more complex magnetic behaviour. A less pronounced kink is also visible for NpBC. The inset shows C_p/T vs. T^2 and the solid line is the fit of $C_p/T = \gamma + \beta T^2$. The Sommerfeld parameter obtained for PuBC, $\gamma = 31$ mJ Pu-mol^{-1} K^{-2}, is almost three times larger than $\gamma = 11.3$ mJ Np-mol^{-1} K^{-2} estimated for NpBC and suggests a much higher density of states at the Fermi energy. The Debye temperature for PuBC, $\Theta_D = 305$ K, is lower than for NpBC and should be taken with caution since the fit was done in a rather high temperature range (4.1 K < T < 9 K).

We were not able to measure the electrical resistivity for the PuBC sample, but the positive slope of $\rho(T)$ ($d\rho/dT > 0$) for NpBC (data not shown here) is in agreement with a non-zero Sommerfeld parameter and confirms the metallic character of NpBC.

To examine theoretically the electronic structure of NpBC and PuBC and to make a comparison with experimental data, we performed spin-polarized local spin density approximation (LSDA) as well as LSDA plus Hubbard U (LSDA+U) calculations, using the experimental lattice parameters and the internal atomic positions listed in Table I.

First, we applied the conventional spin-polarized LSDA, assuming parallel and anti-parallel coupling between two Np moments in the unit cell. Table III reports the calculated spin (μ_S),orbital (μ_L), and total ($\mu = \mu_S + \mu_L$) magnetic moments for the f-states in the "muffin-tin" spheres around Np and Pu atoms (in μ_B units), together with the total energy difference between FM and AFM

TABLE III. Spin (μ_S), orbital (μ_L), and total ($\mu = \mu_S + \mu_L$) magnetic moments for the f-states in the "muffin-tin" spheres around Np and Pu atoms (in μ_B units), together with the total energy difference (eV) between FM and AFM configurations of the magnetic moments in the unit cell.

NpBC		LSDA(+SOC)			FLL-LSDA+U		
Order	Atom	μ_S	μ_L	μ	μ_S	μ_L	μ
FM	Np	1.97	−2.92	−0.95	2.50	−4.35	−1.85
AFM	Np	2.06	−1.89	0.17	2.51	−4.25	−1.74
E(FM)-E(AFM)		−0.136 eV			−0.033 eV		
PuBC		LSDA(+SOC)			FLL-LSDA+U		
Order	Atom	μ_S	μ_L	μ	μ_S	μ_L	μ
FM	Pu	3.48	−1.89	1.59	3.40	−3.72	−0.32
AFM	Pu	3.56	−2.12	1.44	3.35	−3.80	−0.45
E(FM)-E(AFM)		0.087 eV			0.010 eV		

configurations of the magnetic moments in the unit cell. It is seen that LSDA yields a FM ground state for NpBC and a AFM ground state for PuBC. The magnitude of the total magnetization for FM-NpBC (including contributions from the interstitial region) per formula unit (f.u.) of −0.26 μ_B is substantially smaller than the experimental value of 1.14 μ_B. This is attributed to the well-known limitations of LSDA as applied to the actinide materials.

Next, we applied LSDA+U calculations, making use of relativistic (including SOC) LSDA +U.[20] The Coulomb interaction in the Np 5f shell is parameterized by Slater integrals $F_0 = 3.00$ eV, $F_2 = 7.43$ eV, $F_4 = 4.83$ eV, and $F_6 = 3.53$ eV, and $F_0 = 4.00$ eV, $F_2 = 7.76$ eV, $F_4 = 5.05$ eV, and $F_6 = 3.70$ eV for the Pu 5f shell, as given in Ref. 27. They correspond to commonly accepted values for the Coulomb U = 3 eV and the exchange J = 0.61 eV for Np, and U = 4.00 eV and J = 0.64 eV for Pu. Including the Coulomb U and exchange J in the LSDA+U method suggests a FM ground state for NpBC and a AFM ground state for PuBC. Note that the magnitude of the energy difference decreases with the Coulomb U and for the case of PuBC lies near the edge of the numerical accuracy. The total magnetization for FM-NpBC (including contributions from the interstitial region) per formula unit (f.u.) becomes 1.69 μ_B, exceeding somewhat the experimental value of 1.14 μ_B.

The electronic density of states (DOS)—for the FM-ordered NpBC calculated with the fully localized limit FLL-LSDA +U is shown in Figure 6(a), where the total DOS per f.u. is shown together with the MT-sphere projected and spin-[up,dn] resolved DOS for the B- and C-atoms in the unit cell. The DOS in the energy region [−14 eV,−10 eV] is formed mainly by the s-states of B and C. Also, these states are mainly present above the gap at −8 eV. The p-character of the B and C atoms is mostly located at the energies from −5 eV and above. The f-projected and spin-[up,dn] resolved DOS for the Np-atom is shown in Figure 6(b). The DOS spin-polarization is clearly seen with the most of the DOS in the vicinity of the Fermi level coming from the spin-up f-states of Np. The calculated value of the DOS at E_F, $N(E_F) = 1.85$ states/eV corresponds to the Sommerfeld coefficient $\gamma = 4.4$ mJ Np-mol^{-1} K^{-2}, which is smaller than the experimental value.

The DOS for the AFM-ordered PuBC calculated with FLL-LSDA+U is shown in Figure 6(c). The B and C atoms projected DOS character are similar to the NpBC case described above. The f-projected and spin-[up,dn] resolved DOS for the Pu-atom is shown in Figure 6(d). There is a noticeable reduction of $N(E_F)$ to 0.6 states/eV corresponding to a reduced $\gamma = 1.4$ mJ Pu-mol^{-1} K^{-2}.

We have synthesized, characterized crystal structure, and measured physical properties of the two new members of actinoid based borocarbides: NpBC and PuBC. Both compounds are isostructural with the UBC type. As can be seen from Table I, the a and b lattice parameters are almost the same and do not depend on the actinoid element. However, the c lattice parameter increases with the number of electrons of the actinoid atom. The smallest c is observed for UBC (a = 0.334 88(1) nm) and the largest for PuBC (a = 0.339 10(1) nm). As a consequence, the shortest distance between the actinoid atoms increases from 0.3349 for UBC to 0.3380 nm for NpBC, and 0.3391 nm for PuBC.
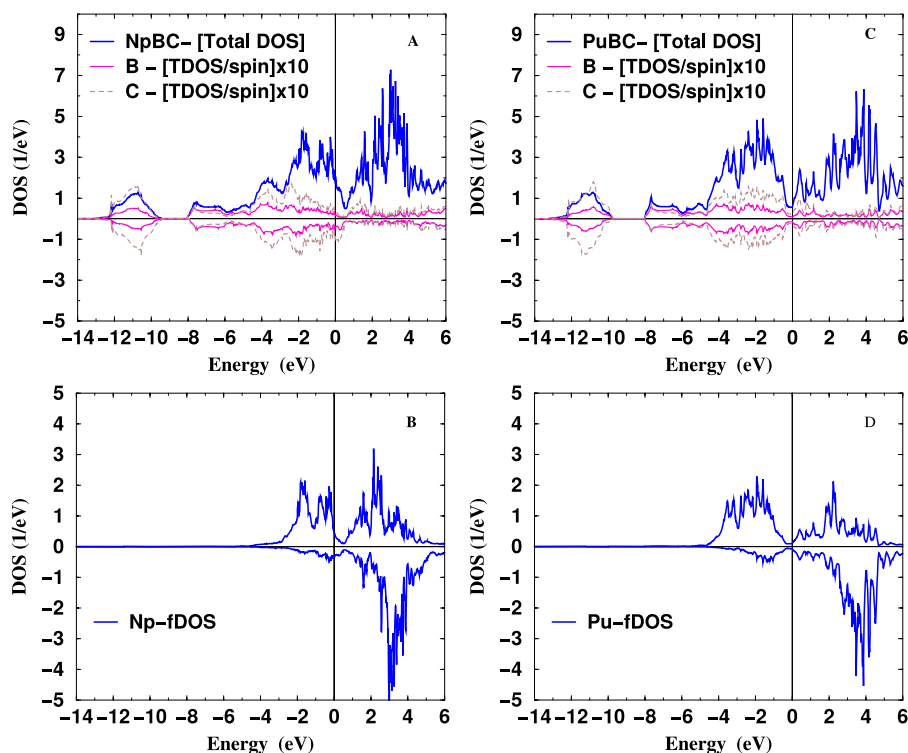
FIG. 6. DOS for NpBC and PuBC: (a) the total DOS/f.u. for NpBC together with spin-up and spin-dn (shown as negative) MT-projected DOS for the B and C atoms; (b) the spin-up and spin-dn (shown as negative) f-projected DOS for the Np atom; (c) the total DOS/f.u. for NpBC together with spin-up and spin-dn (shown as negative) MT-projected DOS for the B and C atoms; (d) the spin-up and spin-dn (shown as negative) f-projected DOS for the Pu atom.

In contrast to the U-based counterpart, which reveals temperature independent paramagnetism, NpBC and PuBC show long range FM and AFM ordering, respectively. This can be qualitatively explained by the idea of Hill—long range magnetic ordering is observed in compounds for which the inter-atomic spacing between actinoid atoms (d_{An-An}) has negligible wave function overlap. Metal-metal distances $d_{Np-Np} = 0.338$ nm for NpBC and $d_{Pu-Pu} = 0.3391$ nm for PuBC are well above 0.325 nm and comparable with 0.34 nm—the critical distance (Hill limit) for Np-Np and Pu-Pu, respectively.[28] However, this simple idea does not predict the type of magnetic ordering and often fails in particular for the Pu containing compounds, for which it was proposed that not the Pu–Pu spacing but rather details of the $5f$ occupancy determine the magnetic ground state.[29–31] In consistency with the experimental results, our electronic structure calculations confirm an FM ground state for NpBC and a AFM ground state for PuBC. A more careful investigation that takes into account hybridization with the ligand atoms is needed to better understand the magnetic behaviour in these systems.

[1] *Handbook on the Physics Chemistry of Rare Earths: Lanthanides/Actinides Physics I*, edited by K. A. Gschneidner, Jr., L. Eyring, and G. H. Choppin (North Holland, 1993), Vol. 17, pp. 1-769.

[2] R. C. Albers, Nature **410**, 759-761 (2001).

[3] A. Toropova, C. A. Marianetti, K. Haule, and G. Kotliar, Phys. Rev. B **76**, 155126 (2007).

[4] Q. Yin, A. Kutepov, K. Haule, G. Kotliar, S. Y. Savrasov, and W. E. Pickett, Phys. Rev. B **84**, 195111 (2011).

[5] T. Klimczuk, H. C. Walker, R. Springell, A. B. Shick, A. H. Hill, P. Gaczyński, K. Gofryk, S. A. J. Kimber, C. Ritter, E. Colineau, J.-C. Griveau, D. Bouexiere, R. Eloirdi, R. J. Cava, and R. Caciuffo, Phys. Rev. B **85**, 174506 (2012).

⁶ T. Klimczuk, A. B. Shick, R. Springell, H. C. Walker, A. H. Hill, E. Colineau, J.-C. Griveau, D. Bouexiere, R. Eloirdi, and R. Caciuffo, Phys. Rev. B **86**, 174510 (2012).

⁷ R. Nagarajan, C. Mazumdar, Z. Hossain, S. K. Dhar, K. V. Gopalakrishnan, L. C. Gupta, C. Godart, B. D. Padalia, and R. Vijayaraghavan, Phys. Rev. Lett. **72**, 274 (1994).

⁸ R.J. Cava *et al.*, Nature **367**, 146 (1994).

⁹ P. C. Canfield, P. L. Gammel, and D. J. Bishop, "New magnetic superconductors: A toy box for solid-state physicists," Phys. Today **51**(10), 40 (1998).

¹⁰ P. Rogl, "Actinoidmetal boron carbides," *The Physics and Chemistry of Carbides, Nitrides and Borides*, edited by R. Freer (Kluwer Academic Publishers, Dordrecht, The Netherlands, 1990), pp. 269-277.

¹¹ P. Rogl, "Ternary System Np-B-C" and "Ternary System Pu-B-C," in *Phase Diagrams of Ternary Metal-Boron-Carbon Systems*, edited by G. Effenberg (ASM-MSI, Materials Park, Ohio, USA, 1998), pp. 230, 244-249.

¹² P. Rogl and P. Fischer, J. Solid State Chem. **90**, 285-290 (1991).

¹³ T. Klimczuk, P. Boulet, J.-C. Griveau, E. Colineau, E. Bauer, M. Falmbig, P. Rogl, and F. Wastin, "Unusual behaviour of $(Np,Pu)B_2C$," Philos. Mag. (published online).

¹⁴ V. H. Tran, P. Rogl, G. Andre, and F. Bouree, J. Phys.: Condens. Matter **18**(2), 703-18 (2006).

¹⁵ V. H. Tran, P. Rogl, D. de Reotier, and A. Yaouanc, Phys. Rev. B **83**, 144417 (2011).

¹⁶ P. Rogl, J. Nucl. Mater. **73**, 198-203 (1978).

¹⁷ P. Rogl, B. Rupp, I. Felner, and P. Fischer, J. Solid State Chem. **104**, 377-390 (1993).

¹⁸ F. Jutier, G. A. Ummarino, J.-C. Griveau, F. Wastin, E. Colineau, J. Rebizant, N. Magnani, and R. Caciuffo, Phys. Rev. B **77**, 024521 (2008).

¹⁹ T. Roisnel and J. Rodriguez-Carvajal, Mater. Sci. Forum **378-381**, 118 (2001).

²⁰ A. B. Shick, D. L. Novikov, and A. J. Freeman, Phys. Rev. B **56**, R14259 (1997).

²¹ A. B. Shick and W. E. Pickett, Phys. Rev. Lett. **86**, 300 (2001).

²² W. D. Callister, Jr., *Materials Science and Engineering: An Introduction*, 6th ed. (John Wiley & Sons, Inc., 2003), p. 693.

²³ M. D. Le, K. A. Mcewen, E. Colineau, J.-C. Griveau, and R. Eloirdi, Phys. Rev. B **82**, 155136 (2010).

²⁴ A. Tari, *The Specific Heat of Master at Low Temperatures* (Imperial College Press, London, 2003), pp. 149-150.

²⁵ E. Colineau, P. Javorsky, P. Boulet, F. Wastin, J. C. Griveau, J. Rebizant, J. P. Sanchez, and G. R. Stewart, Phys. Rev. B **69**, 184411 (2004).

²⁶ T. Klimczuk, J.-C. Griveau, P. Gaczynski, R. Eloirdi, E. Colineau, and R. Caciuffo, J. Phys.: Conf. Ser. **273**, 012024 (2011).

²⁷ K. T. Moore and G. van der Laan, Rev. Mod. Phys. **81**, 235 (2009).

²⁸ H. H. Hill, *Proceedings of 4th International Conference on Plutonium and other Actinides, Santa Fe, NM, 1970*, edited by W. N. Miner (Nuclear Metallurgy, 1970), Vol. 17, p. 2.

²⁹ L. Havela, A. Shick, and T. Gouder, J. Appl. Phys. **105**, 07E130 (2009).

³⁰ T. Gouder, L. Havela, A. B. Shick, F. Huber, F. Wastin, and J. Rebizant, J. Phys.: Condens. Matter **19**, 476201 (2007).

³¹ L. Havela, P. Javorský, F. Wastin, E. Colineau, T. Gouder, A. B. Shick, and V. Drchal, J. Alloys Compd. **444–445**, 88-92 (2007).

³² E. Parthé, L. Gelato, B. Chabot, M. Penzo, K. Cenzual, and R. Gladyshevskii, *TYPIX Standardized Data and Crystal Chemical Characterization of Inorganic Structure Types* (Springer, Berlin, Heidelberg, 1994).